



Higher CO₂ Assimilation in Selected Rice Recombinant Inbred Lines Is Driven by Higher CO₂ Diffusion and Light Use Efficiency Related to Leaf Anatomy and Mesophyll Cell Density

OPEN ACCESS

Faliang Zeng, Lin Zhu, Guojiao Wang, Yinpei Liang, Dianrong Ma* and Jiayu Wang*

Edited by:Alistair McCormick,
The University of Edinburgh,
United Kingdom**Reviewed by:**Hiroki Ikawa,
Hokkaido Agricultural Research
Center, National Agriculture and Food
Research Organization, Japan
Aihua Sha,
Yangtze University, China***Correspondence:**Dianrong Ma
madianrong@syau.edu.cn
Jiayu Wang
wangjiayu@syau.edu.cn**Specialty section:**This article was submitted to
Plant Physiology,
a section of the journal
Frontiers in Plant Science**Received:** 07 April 2022**Accepted:** 04 May 2022**Published:** 09 June 2022**Citation:**Zeng F, Zhu L, Wang G, Liang Y,
Ma D and Wang J (2022) Higher CO₂
Assimilation in Selected Rice
Recombinant Inbred Lines Is Driven
by Higher CO₂ Diffusion and Light
Use Efficiency Related to Leaf
Anatomy and Mesophyll Cell Density.
Front. Plant Sci. 13:915050.
doi: 10.3389/fpls.2022.915050

Key Laboratory of Rice Biology & Genetic Breeding in Northeast China (Ministry of Agriculture and Rural Areas), Rice Research Institute, Shenyang Agricultural University, Shenyang, China

Leaf anatomy determining the light distribution within the leaf and exerting influence on CO₂ diffusion is considered to have dramatic potential for photosynthesis performance increase. In this study, we observed that two rice recombinant inbred lines, H138 and H217 (RILF₁₁ plants from Sasanishiki × IRAT10), have higher net CO₂ assimilation (A_n) than their parent Sasanishiki due mainly to the improvement of leaf anatomy. Our results showed that A_n positively correlated with anatomy traits' mesophyll cell number per cross-sectional area (NO_{mes}cell/A_{cross}) and mesophyll area (A_{mes}). NO_{mes}cell/A_{cross} exert direct and indirect effects on A_n. Compared to Sasanishiki flag leaves, IRAT10, H138, and H217 have higher mesophyll cell numbers. Simultaneously, higher chlorophyll content and expression of genes encoding the light-harvesting protein of PSII and PSI (*Lhcb1*, 2, 3 and *Lhca1*, 2, 3) were recorded in IRAT10, H138, and H217, which facilitates light use efficiency. Higher electron transport rate and RuBP concentration were recorded in IRAT10, H138, and H217 flag leaves. Retinoblastoma-related gene (*OsRBR1*), exerting effects on mesophyll cell density, can be used to modify leaf anatomy for improving leaf photosynthesis. Additionally, higher stomatal conductance and mesophyll conductance were also recorded in H138 and H217 than in Sasanishiki. Furthermore, we modeled mesophyll conductance through anatomical traits, and the results revealed that chloroplast thickness was the dominant factor restricting CO₂ diffusion within mesophyll cells rather than cell wall thickness. Higher RuBP content accompanied by higher CO₂ concentration within the carboxylation set in H138 and H217 flag leaves contributed to higher CO₂ assimilation.

Keywords: leaf anatomy, CO₂ diffusion, stomatal conductance, mesophyll conductance, electron transport rate, mesophyll cell number, photosynthesis

INTRODUCTION

Rice is an important food crop, and its yield mainly derives from the accumulation of photosynthetic substances in leaves after the heading stage. Photosynthesis, a key factor in the formation of rice yields, contributed little to rice productivity gains over the past half-century (Zhu et al., 2010). Improving the photosynthetic efficiency of crop leaves has been considered an important and effective strategy for increasing crop yield potential and productivity (Zhu et al., 2010; Lawson et al., 2012; Ort et al., 2015; Simkin et al., 2019). Leaf anatomy determining the light distribution within the leaf and exerting dramatic influence on CO₂ diffusion is considered to have dramatic potential on the enhance of photosynthetic capacity (Zhang et al., 2014; He et al., 2017; Lehmeier et al., 2017). Thicker leaves with more and small mesophyll cells could increase mesophyll conductance (g_m), which contributes to a higher photosynthesis rate (He et al., 2017). Meanwhile, wild rice with fewer larger mesophyll cells between two minor veins, but with more chloroplasts in a mesophyll cell, contributed to higher photosynthetic efficiency (Mathan et al., 2021). Both larger and smaller mesophyll cells increase the net photosynthetic rate in Arabidopsis, while the mechanism of photosynthesis enhancement differs in different mesophyll cell sizes (Barroco et al., 2006; Lehmeier et al., 2017). Additionally, rice with *Narrow leaf1* (*NAL1*) genes changed the arrangement of vascular bundles in leaves and narrowed the leaves, which achieved higher photosynthesis efficiency (Zhang et al., 2014). Hence, the precise target for engineering leaf anatomy still needs to be further studied.

Accordingly, CO₂ diffusion within the leaf can be divided into stomatal diffusion and mesophyll diffusion. Stomatal diffusion mainly refers to the diffusion of CO₂ moving from the atmosphere to the sub-stomatal internal cavities through the stomatal pores. Mesophyll diffusion refers to the diffusion of CO₂ moving from sub-stomatal internal cavities to the outside the mesophyll cell wall (gas phase diffusion), and from there to the site of carboxylation inside the stroma through the cell wall, plasma membrane, cytoplasm, chloroplast envelope membranes and stroma (liquid phase diffusion) (Evans et al., 1994, 2009). Mesophyll conductance has been recognized as a crucial limitation, and even the most consistent limitation of photosynthesis in some species (Tosens et al., 2012a,b; Peguero-Pina et al., 2017; Xiong et al., 2017; Xiong and Flexas, 2018; Han et al., 2018; Ren et al., 2019; Flexas et al., 2021). However, g_m varied across species, even the same species between genotypes mainly linked to anatomical properties (Tomas et al., 2013; He et al., 2017; Ouyang et al., 2017; Peguero-Pina et al., 2017). Among leaf anatomical traits, mesophyll cell wall thickness (T_{cw}) and the total chloroplast surface area exposed to mesophyll intercellular air spaces per leaf area (S_C/S) are the two strongest anatomical limitations to the maximum g_m (Tomas et al., 2013; Evans, 2021). The cell wall thickness strongly and negatively correlates with g_m and A_n , and limitations derived from S_C/S are frequently equal to or smaller than T_{cw} (Flexas et al., 2021). High S_C/S means more chloroplast exposed to CO₂, which can improve CO₂ concentration at the sites of carboxylation by a great level (He et al., 2017). However, a recent study showed that

T_{cw} and S_C/S seemed to be varied independently, and the two factors compensate for each other to achieve the maximum g_m in some cases (Peguero-Pina et al., 2017). Moreover, in cotton leaves, T_{cw} is the dominant factor restricting g_m in palisade tissue cells, while chloroplast thickness (T_{chl}) is the main liquid component restricting g_m in the sponge tissue (Han et al., 2018). Furthermore, the drought did increase T_{cw} of rice but was not followed by a decrease in g_m , which might indicate that T_{cw} was not the dominant limiting factor for g_m under water stress (Ouyang et al., 2017). This view has not been proven yet. Hence, the dominant liquid factor restricting CO₂ diffusion in rice still needs to be researched.

Under the field condition, we found that IRAT10 with thicker leaves has a higher photosynthetic rate than Sasanishiki, which may be benefited from leaf anatomy traits. Additionally, H138 and H217 from the recombinant inbred line of IRAT10 × Sasanishiki have higher photosynthetic rates than their parent Sasanishiki. We suspect that the increase in photosynthetic efficiency of H138 and H217 might be related to the leaf anatomical traits inherited from their parent IRAT10. This has great significance for rice breeding. It makes sense to investigate the mechanism of photosynthetic improvements benefited from CO₂ diffusion or biochemical factors mediated by leaf anatomy traits. In addition, we modeled mesophyll conductance from anatomical traits to reveal the dominant components that restrict CO₂ diffusion and make up for the lack of application of the methods in rice.

MATERIALS AND METHODS

Plant Material and Grown Condition

Sasanishiki (*Oryza sativa japonica* subspecies) and IRAT10 (*O. sativa japonica* subspecies, upland), as well as two recombinant inbred lines, H138 and H217 (RILF11 plants from Sasanishiki × IRAT10), were used in this study. The genetic map of tested materials is shown in **Supplementary Figure 1**. Seeds were pre-germinated and grown in a nursery for four weeks, and then the seedlings were transplanted into 11-L plots, containing 10-kg paddy soil, with a density of two plants per hill and two hills per pot. Fertilizers, weeds, pests, and diseases were controlled the same with the field to avoid a yield loss. For each genotype, 40 pots were planted. At the heading stage (14 days after flag leaves full expansion, on August 3, 2020), the fully expanded flag leaves on the main stem were sampled and measured on the same day to identify the difference between the two cultivars on photosynthesis performance. The heading stage of the tested varieties was almost the same.

Chlorophyll Content, Gas Exchange, and Chlorophyll Fluorescence

Chlorophyll was extracted from flag leaves in 20 ml of 95% alcohol for 48 h at room temperature under a dark environment according to the method described by Sartory and Grobbelaar (1984). The absorbances of the extract under 665 and 649 nm were determined using a spectrophotometer. Chlorophyll content were calculated with the following equations: chlorophyll

a ($\mu\text{g mL}^{-1}$) = $13.95 (A_{665}) - 6.88 (A_{649})$, chlorophyll b ($\mu\text{g mL}^{-1}$) = $24.96 (A_{649}) - 7.32 (A_{665})$. The total chlorophyll content is the sum content of chlorophyll a and chlorophyll b . For each genotype, six biological replicates were measured.

A portable infrared gas analyzer (CIRAS3, PP Systems, Amesbury, MA, United States) equipped with an integrated leaf fluorometer head (CFM3, PP Systems) was used to measure gas exchange and chlorophyll fluorescence parameters simultaneously on a sunny day. About nine flag leaves on the main stem of each genotype were selected to exert gas exchange measurement. The photon flux density (PPFD) in the leaf chamber was maintained at $1,200 \mu\text{mol m}^{-2} \text{s}^{-1}$ provided by a LED source with a light ratio of red: green: blue: white 90: 0: 5: 5%. CO_2 concentration in the leaf chamber was maintained at $400 \mu\text{mol mol}^{-1}$ provided by a CO_2 injector system. The leaf temperature in the chamber was controlled at 25°C , and the flow rate was controlled at $200 \mu\text{mol s}^{-1}$. Net CO_2 assimilation (A_n , $\mu\text{mol m}^{-2} \text{s}^{-1}$), internal CO_2 concentration (C_i , $\mu\text{mol mol}^{-1}$), and stomatal conductance (g_s , $\text{mmol m}^{-2} \text{s}^{-1}$) were recorded simultaneously when the system stabilized to a steady-state. Then, a fluorometric procedure was performed to measure the steady-state fluorescence (F_s) and maximum fluorescence (F_m'). The saturating light pulse was $8,000 \mu\text{mol m}^{-2} \text{s}^{-1}$. The actual photochemical efficiency of photosystem II (ΦPSII) was calculated with the following equations:

$$\Phi\text{PSII} = \frac{F_m' - F_s}{F_m'} \quad (1)$$

The electron transport rate (J) was calculated as:

$$J = \Phi\text{PSII} \times \text{PPFD} \times \alpha \times \beta \quad (2)$$

where α refers to the leaf absorbance, and β is the distribution of electrons between the photosynthetic system I (PSI) and PSII. Previously, α was assumed as 0.85, and β was assumed as 0.5 between PSI and PSII (Manter and Kerrigan, 2004; Li et al., 2009; Gilbert et al., 2012). In this paper, α and β were estimated from a light response curve under a gradient of PPFD of 400, 200, 100, and $0 \mu\text{mol m}^{-2} \text{s}^{-1}$ at low O_2 concentrations (<2%). The slope of the relationship between ΦPSII and $4\Phi\text{CO}_2$ (the quantum efficiency of CO_2 uptake) was taken as the value of $\alpha\beta$ (Valentini et al., 1995).

The mesophyll conductance of CO_2 (g_m) was determined as the following equation described by Harley et al. (1992):

$$g_m = \frac{A}{C_i \times \frac{\Gamma^* \times (J + 8(A + R_d))}{J - 4(A + R_d)}} \quad (3)$$

where Γ^* refers to the CO_2 compensation point in the absence of photorespiration, and R_d is the respiration in the daytime. Γ^* and R_d were estimated from A/C_i curves, and CO_2 concentrations in the leaf chamber were set in a series of 200, 150, 100, 75, and $50 \mu\text{mol mol}^{-1}$, under three light intensities (300, 200, and $100 \mu\text{mol m}^{-2} \text{s}^{-1}$) and low O_2 concentrations (<2%) (Li et al., 2009) (Pons et al., 2009). The coordinate of the intersection of the three A/C_i curves represented R_d and Γ^* (Li et al., 2009;

Pons et al., 2009). CO_2 leakage was measured to make the gas exchange measurement more accurate (Flexas et al., 2007).

Analysis of Leaf Morphological and Anatomical Characters

Nine flag leaves on the main stem of each genotype were graphed to measure leaf length, leaf width, and leaf area using Image J software (National Institutes of Health, Bethesda, MD, United States). Dry weights were determined when the flag leaves were dried to a constant weight at 80°C for 48 h. Leaf mass per area (LMA) is the ratio of dry weight and leaf area. Then the dried samples were used for nitrogen concentration determination through a carbon and nitrogen analyzer (MT700 Mark II; Yanako).

For light microscopy, leaf sections (approximately 1 cm in length) from the middle of leaves were collected with the formalin acetic-alcohol solution. Samples were dehydrated with ethanol series (50, 70, 80, 95, and 100%) and then, were embedded with paraffin (melting point $56\text{--}58$ degrees). A sliding microtome (Leica RM2255) was used to cut the block into transverse sections $7 \mu\text{m}$ in thickness. Light sections were stained using 1% toluidine blue, then the sections were scanned under a digital whole slide scanning. Anatomical characteristics were determined using CaseViewer.

The thickness of leaf/mesophyll ($T_{\text{leaf}}/T_{\text{mes}}$, μm), the cross-sectional area of each mesophyll cell (A_{cell} , μm^2), the ratio of mesophyll cell (A_{mes}), bulliform cell (A_{bf}), main vein ($A_{\text{main vein}}$), major vein ($A_{\text{maj vein}}$), and minor vein ($A_{\text{min vein}}$) area to cross-sectional area (A_{cros}), and the lengths between two neighboring major/minor vascular bundle ($L_{\text{major vein}}/L_{\text{minor vein}}$, μm), were determined. Mesophyll cell number per cross-sectional area ($\text{NO}_{\text{mes cell}}/A_{\text{cros}}$, number μm^{-2}) was calculated as a quotient of dividing A_{mes} by A_{cell} . The cross-sectional areas of >30 mesophyll cells were measured between the vascular bundles. For each genotype, at least six leaf sections from flag leaves of different main stems were used for anatomical character measurement.

Electron Microscope and Estimate G_m From Anatomical Characteristics

Leaf pieces between the first and the second major vein (approximately $4 \text{ mm} \times 1 \text{ mm}$) from the same leaves used for light microscopy were cut and immersed in 0.1 M phosphate buffer (pH 7.2) with 2.5% glutaric aldehyde and 3% paraformaldehyde under vacuum for 48 h. Then, the leaf pieces were further fixed in 1% osmium tetroxide for another 2 h, followed by washing three times with phosphate buffer. Then, an ethanol series was used to dehydrate leaf pieces. After dehydration, the leaf samples were embedded in resin for ultrathin sections. Ultrathin sections were further stained with 7.7% uranyl acetate (30 min) and lead citrate (4 min) for photographing under an electron microscope (TEM HT770, Hitachi, Japan). Chloroplast length (L_{chl}), chloroplast thickness (T_{chl}), and the cross-sectional area of chloroplast (A_{chl}) were measured at $1,200\text{--}1,500\times$ magnification. Mesophyll cell wall thickness (T_{cw}) and cytoplasm thickness (T_{cyt}) were measured at $12,000\times$ magnification. For each genotype, six-leaf sections from

different plants were used. For each section, three different view fields were measured.

The fraction of intercellular airspace (f_{ias}) was determined as (Tomas et al., 2013):

$$f_{ias} = 1 - \frac{\sum S_s}{T_{mes} \times W} \quad (4)$$

where $\sum S_s$ is the total area of mesophyll cells in the section, T_{mes} refers to the mesophyll thickness between epidermal layers, W is the section width, and all measurements were performed at $800\times$ magnification.

The surface area of mesophyll and chloroplasts exposed to the intercellular airspaces (S_m/S and S_c/S) were calculated as follows (Evans et al., 1994; Scafaro et al., 2011):

$$S_m = \frac{L_m}{W} F \quad (5)$$

$$S_c = \frac{L_c}{W} F \quad (6)$$

The L_m and L_c refer to the length of mesophyll and chloroplast exposed to the intercellular airspace (μm). F is the curvature correction factor and was taken as 1.55 in rice (Syvertsen et al., 2010).

A one-dimensional gas diffusion model was used to estimate mesophyll conductance from anatomical characteristics ($g_{m\text{ ana}}$) (Niinemets, 2003; Tosens et al., 2012a,b). In this model, mesophyll conductance is divided into gas-phase conductance and liquid-phase conductance.

$$g_{m\text{ ana}} = \frac{1}{\frac{1}{g_{ias}} + \frac{RT_k}{H \cdot g_{liq}}} \quad (7)$$

where g_{ias} is the gas phase conductance that links to CO_2 moving from substomatal internal cavities to the outer surface of the mesophyll cell wall, and g_{liq} is the liquid phase conductance that links to CO_2 moving from the outer surface of cell walls to the stroma. Gas constant (R , $\text{Pa m}^3 \text{K}^{-1} \text{mol}^{-1}$), Henry's law constant (H , $\text{Pa m}^3 \text{mol}^{-1}$), and absolute temperature (T_k ,

K) were used to convert g_{liq} to gas equivalent conductance (Niinemets, 2003).

The gas-phase conductance (g_{ias}) is determined as (Niinemets, 2003):

$$g_{ias} = \frac{D_a \times f_{ias}}{\Delta L_{ias} \times \zeta} \quad (8)$$

where ζ , the diffusion path tortuosity, was assumed as 1.57 (mm^{-1}); and D_a , the diffusion coefficient for CO_2 in the gas phase, was assumed as 1.51×10^{-5} ($\text{m}^2 \text{s}^{-1}$ at 25°C); ΔL_{ias} , the average gas-phase thickness, was assumed as half of the mesophyll thickness between epidermal layers.

The total liquid phase conductance is the sum conductance of each component including cell wall (g_{cw}), plasmalemma (g_{pl}), cytosol (g_{cyt}), chloroplast envelope (g_{en}), and chloroplast stroma (g_{st}).

$$\frac{1}{g_{liq}} = \left(\frac{1}{g_{cw}} + \frac{1}{g_{pl}} + \frac{1}{g_{cyt}} + \frac{1}{g_{en}} + \frac{1}{g_{st}} \right) \times \frac{S_c}{S} \quad (9)$$

The conductance of the mesophyll cell wall, cytosol, and chloroplast can be estimated from a general equation (Tosens et al., 2012a,b).

$$the\ g_i = \frac{r_{f,i} \times D_w \times p_i}{\Delta L_i} \quad (10)$$

where dimensionless factor $r_{f,i}$ is the reduction of diffusion conductance in corresponding components relative to free diffusion in water. The $r_{f,i}$ approximate to 1 for cell wall, and 0.3 for g_{cyt} and g_{st} . D_w , the aqueous phase diffusion coefficient for CO_2 , was 1.79×10^{-9} ($\text{m}^2 \text{s}^{-1}$) at 25°C . ΔL_i (m) is the corresponding thickness of each component in the CO_2 diffusion pathways. The effective porosity (p_i , $\text{m}^3 \text{m}^{-3}$) in cytosol and chloroplast was taken as 1. Cell wall porosity (p_{cw}) was calculated from T_{cw} ($p_{cw} = -0.3733 \times T_{cw} + 0.3378$) (Tosens et al., 2016). Both g_{pl} and g_{en} were assumed as 0.0035 ms^{-1} (Evans et al., 1994; Tosens et al., 2012a,b). Conductance units in the form of m s^{-1} were converted into molar units according to the equation $g[\text{mol m}^{-2} \text{s}^{-1}] = g[\text{ms}^{-1}] \times 44.6 \times 273.15/(273.15$

TABLE 1 | Leaf length (L_l , cm), leaf width (L_w , cm), leaf area (A_{leaf} , cm^2), leaf mass per unit area (LMA, mg cm^{-2}), the distance between two major veins ($L_{\text{majorvein}}$, μm), the distance between two minor veins ($L_{\text{minorvein}}$, μm), the cross-area of a single mesophyll cell (A_{mescell} , μm^2), the mesophyll cell number per cross-sectional area ($\text{NO}_{\text{mes}}/A_{\text{cross}}$), leaf thickness (T_{leaf} , μm), and mesophyll thickness (T_{mes} , μm) in the flag leaves of the tested varieties.

	IRAT10	Sasanishiki	H138	H217
L_l (cm)	25.13 \pm 2.03b	29.69 \pm 2.38a	23.51 \pm 2.58c	21.08 \pm 2.9c
L_w (cm)	1.59 \pm 0.06b	1.22 \pm 0.07d	1.44 \pm 0.05c	1.74 \pm 0.11a
A_{leaf} (cm^2)	25.961 \pm 2.35a	23.66 \pm 3.31b	22.12 \pm 2.92b	23.75 \pm 3.01b
LMA (mg cm^{-2})	6.76 \pm 0.16a	5.39 \pm 0.16c	5.88 \pm 0.13b	5.33 \pm 0.07c
Ames cell (μm^2)	249 \pm 13.4a	203 \pm 7.1b	157 \pm 6.5c	199 \pm 4.7b
$\text{NO}_{\text{mes}} \text{ cell}/A_{\text{cross}}$	7293 \pm 169b	4565 \pm 161c	7537 \pm 332b	8120 \pm 344a
$L_{\text{majorvein}}$ (μm)	1304 \pm 12.5c	1370 \pm 20.5b	1294 \pm 56.8c	1622 \pm 75.3a
$L_{\text{minorvein}}$ (μm)	217 \pm 14.4b	213 \pm 4.8b	184 \pm 2.5c	276 \pm 0.9a
T_{leaf} (μm)	182 \pm 5.79a	100 \pm 0.63d	122 \pm 2.4b	115 \pm 1.8c
T_{mes} (μm)	128.91 \pm 0.76a	64.16 \pm 0.57d	79.57 \pm 2.45b	73.03 \pm 1.23c

Different letters in the same row indicate significant statistical differences among tested varieties at the 0.05 probability level.

+ T_{emL}) \times (P/101.325), where T_{emL} is the leaf temperature ($^{\circ}C$) and P (Pa) is the air pressure (Tosens et al., 2012a).

$$Lm_i = \frac{g_{m_{ana}}}{g_i \times \frac{S_c}{S}} \quad (12)$$

where Lm_{ias} refers to the limitation derived from the gas phase component, Lm_i refers to the limitation of the cell wall, plasmalemma, cytoplasm, chloroplast envelope, and stroma.

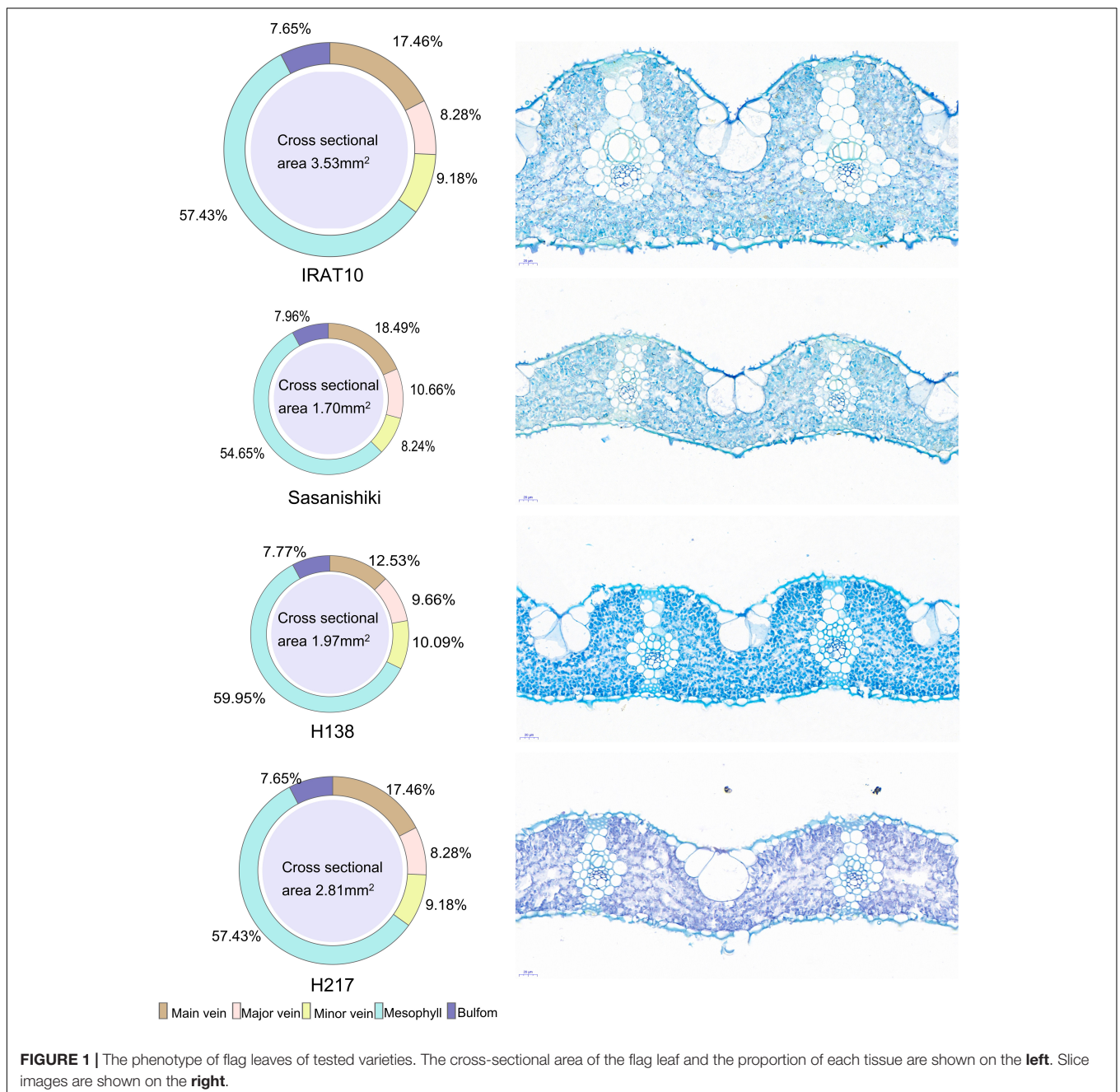
Limitation Analysis of Different Components of g_m

Limitations of each component involved in CO_2 diffusion pathways were calculated as (Tosens et al., 2016):

$$Lm_{ias} = \frac{g_{m_{ana}}}{g_{ias}} \quad (11)$$

Stomatal Morphological Traits and the Maximum Stomatal Conductance

Another two leaf sections (approximately 5 mm \times 5 mm) from the same leaf used for anatomical measurements were collected



with the fixative 2.5% glutaric aldehyde in 0.1 mol L⁻¹ phosphate buffer (pH 7.6) under dark for 48 h. Then, the leaf samples were washed three times with phosphate buffer. After an ethanol series and a tertButanol series, the samples were freeze-dried. Images were photographed using a scanning electron microscope (HITACHI Regulus 8100). At least three views on abaxial and adaxial sides were photographed from one section, and at least six leaves from different plants were used for each genotype. Stomatal density (SD, NO. mm²), stomatal length (L_S, μm), and stomatal width (W_S, μm) on each leaf side was measured using ImageJ. The stomatal size was determined by the maximum area of the open stomatal pore (a_{max}, μm²) calculated as described in Ouyang et al. (2017).

$$a_{max} = \frac{(L_S \times W_S \times \pi)}{4} \quad (13)$$

Maximum theoretical stomatal diffusive conductance (g_{S max}) can be estimated according to,

$$g_{S max} = \frac{d \times SD \times a_{max}}{1.6 \times v \times (l + \frac{\pi}{2} \times \sqrt{\frac{a_{max}}{\pi}})} \quad (14)$$

where *d* is the diffusivity of water vapor in the air (24.9 × 10⁻⁶ m² s⁻¹, at 25°C), *v* is the molar volume of air (22.4 × 10⁻³ m³ mol⁻¹, at 25°C), and *l* is the stomatal pore depth for fully open stomata, which assumed to be equal to the width of stomatal guard cell. The g_{Smax} is the sum of abaxial and adaxial conductance.

Quantitation of Content and Activity of Carbon Fixation Related Enzyme

After the gas exchange measurement flag leaves on the main stem were collected and stored at -80°C until to determine the biochemical indices. For each genotype, six biological replicates were measured. The contents of RuBP, Rubisco, PGA (3-phosphoglycerate), and the activity of Rubisco were measured using commercial ELISA kits following the manufacturer's instructions (Jiangsu Meimian industrial Co., Ltd.).

Total RNA Extraction and Real-Time Quantitative PCR Analysis

Flag leaves of tested varieties (4 varieties × 3 biological replicates) were used for total RNA isolation using MiniBEST Plant RNA Extraction Kit (TaKaRa, Dalian, China). Then, total RNA was used for complementary DNA (cDNA) library construction. Real-time PCR was performed on an Applied Biosystems QuantStudio 3 Real-Time PCR System (Thermo Fisher Scientific, United States) using TB Green® Premix Ex Taq™ II (Tli RNaseH Plus) (TaKaRa, Dalian, China). Genes related to photosynthesis were checked, and the sequences of primers are shown in **Supplementary Table 1**. The relative expression of genes was calculated through method Livak and Schmittgen (2001).

RNA-Sequencing

Flag leaves of tested varieties (4 varieties × 3 biological replicates) were used for total RNA isolation on the same day after gas exchange measurements. Total RNA was isolated for cDNA library construction. The cDNA libraries were sequenced using Illumina HiSeq™ 2500 sequencing platform (Illumina Crop., San Diego, CA, United States) by MetWare (MetWare Biotechnology Co., Ltd., Wuhan, China). After filtrating the adapter and low-quality reads, clean reads were aligned to the reference genome Nipponbare *O. sativa ssp. japonica*¹ by DESeq2 (Love et al., 2014; Varet et al., 2016), and the expression abundance was calculated by featureCounts (Liao et al., 2014). Genes with an expression |Log2 Fold Change| ≥ 1 and FDR < .05 were considered as differentially expressed genes (DEGs). Then, DEGs were subjected to enrichment analysis of the clusters of orthologous groups of proteins (KOG data base were used) function and Kyoto Encyclopedia of Genes and Genomes (KEGG) pathway.

Statistical Analysis

One-way analysis of variance (ANOVA) was used to test the statistically significant differences among tested varieties,

¹<https://rapdb.dna.affrc.go.jp/index.html>

TABLE 2 | The cross-sectional area of chloroplast (A_{chl}, μm²), the chloroplast thickness (T_{chl}, μm), the chloroplast length (L_{chl}, μm), the number of chloroplast per mesophyll cell (NO_{chl}/Cell), the thickness of the cytoplasm between the cell membrane and the chloroplast (T_{cyt}, μm), mesophyll cell wall thickness (T_{cw}, μm), the surface of mesophyll cells and chloroplasts exposed to leaf intercellular air spaces (Sm/S and Sc/S, μm² μm⁻²), the volume fraction of intercellular air space (f_{ias}, %), and gm modeled from anatomical traits (g_{m ana}, mol m⁻² s⁻¹) in the flag leaves of tested varieties.

	IRAT10	Sasanishiki	H138	H217
A _{chl} (μm ²)	10.04 ± 3.11bc	15.15 ± 4.88a	11.42 ± 3.70b	9.42 ± 3.68c
T _{chl} (μm)	2.31 ± 0.44b	3.15 ± 0.74a	2.55 ± 0.75b	2.32 ± 0.68b
L _{chl} (μm)	5.34 ± 1.07a	5.20 ± 1.29ab	5.29 ± 0.97a	4.69 ± 0.95b
NO _{chl} /Cell	8.8 ± 1.12a	8.3 ± 1.9a	8.6 ± 1.1a	8.4 ± 1.0a
T _{cyt} (μm)	0.161 ± 0.041a	0.110 ± 0.036b	0.134 ± 0.052b	0.178 ± 0.059a
T _{cw} (μm)	0.189 ± 0.035b	0.224 ± 0.072a	0.216 ± 0.055ab	0.238 ± 0.053a
Sm/S	6.08 ± 0.82c	7.41 ± 1.0a	7.28 ± 0.60a	6.69 ± 0.11b
Sc/S	4.48 ± 0.99d	7.13 ± 0.88a	6.24 ± 0.78a	6.08 ± 0.35a
f _{ias} (%)	6.95 ± 1.49c	11.29 ± 1.81b	10.22 ± 1.38b	14.84 ± 1.88a
g _{m ana} (mol m ⁻² s ⁻¹)	0.108 ± 0.003a	0.081 ± 0.001c	0.097 ± 0.003b	0.104 ± 0.003a

Different letters in the same row indicate significant statistical differences among tested varieties at the 0.05 probability level.

which was performed through SPSS 22.0 software (IBM Inc.). Multivariate correlation analysis was used to reveal the relationship between leaf anatomical traits and photosynthetic parameters. Structural equation modeling (SEM) was performed to determine the causal relationships between leaf anatomy and photosynthetic capacity, which was exerted with AMOS 22.0.0 software.

RESULTS

Leaf Anatomical Traits

Sasanishiki flag leaves have the longest leaf length (21.08 cm) and H217 has the shortest (29.69 cm) (Table 1). Contrary to leaf length, Sasanishiki flag leaves leaf width was the narrowest (1.22 cm), and H217 was the widest (1.74 cm) among tested varieties. Compared to Sasanishiki, H138, and H217, leaf area and leaf mass per area in IRAT10 flag leaves were the largest (25.96 cm², 6.76 mg cm⁻²). Much longer distances between two neighboring major veins or minor veins ($L_{\text{major vein}}/L_{\text{minor vein}}$) were observed in H217 (1622, 276 μm) flag leaves. The cross-area of a single mesophyll cell varied from 157 to 249 μm², with IRAT10 having the largest and H138 having the smallest. Leaf thickness and the mesophyll thickness of IRAT10 (182, 128 μm), H138 (122, 79.57 μm), and H217 (115, 73.03 μm) flag leaves were significantly thicker than that of Sasanishiki (100, 64.16 μm). The cross-sectional area, the proportion of mesophyll cell area accounts for the cross-sectional area, and mesophyll cell number per cross-sectional area of flag leaves in IRAT10, H138, and H217 were significantly higher than that in Sasanishiki (Figure 1 and Table 1).

Chloroplast cross-sectional area (A_{chl}) and chloroplast thickness (T_{chl}) in Sasanishiki flag leaves (15.15 μm², 3.15 μm) were significantly higher than that of IRAT10, H138, and H217 (Table 2 and Supplementary Figure 2). Chloroplast length (L_{chl}) in flag leaves of IRAT10, Sasanishiki, and H138 was 13.8, 10.9, and 12.8% larger than H217 (4.69 μm), respectively. The significantly bigger A_{chl} of Sasanishiki flag leaves was mainly due to the thicker chloroplast thickness (T_{chl}), and shorter L_{chl} contributed to a smaller A_{chl} in H217 flag leaves. The number of chloroplast per mesophyll cell ($\text{NO}_{\text{chl}}/\text{Cell}$) has no difference among tested varieties. Cytoplasm thickness (T_{cyt}) of IRAT10 (0.161 μm) and H217 (0.178 μm) were significantly higher than Sasanishiki (0.110 μm) and H138 (0.134 μm). Compared to Sasanishiki (0.224 μm) and H217 (0.238 μm), IRAT10 (0.189 μm) and H138 (0.216 μm) have a thinner cell wall thickness (T_{cw}). The surface area of mesophyll and chloroplasts exposed to the intercellular airspaces ($S_{\text{m/S}}$ and $S_{\text{c/S}}$) and the fraction of intercellular airspace of Sasanishiki, H138, and H217 were significantly higher than that of IRAT10 (6.08, 4.48 μm² μm⁻², 6.95%).

Conductance of CO₂ Diffusion Through Stomatal and Mesophyll Cell

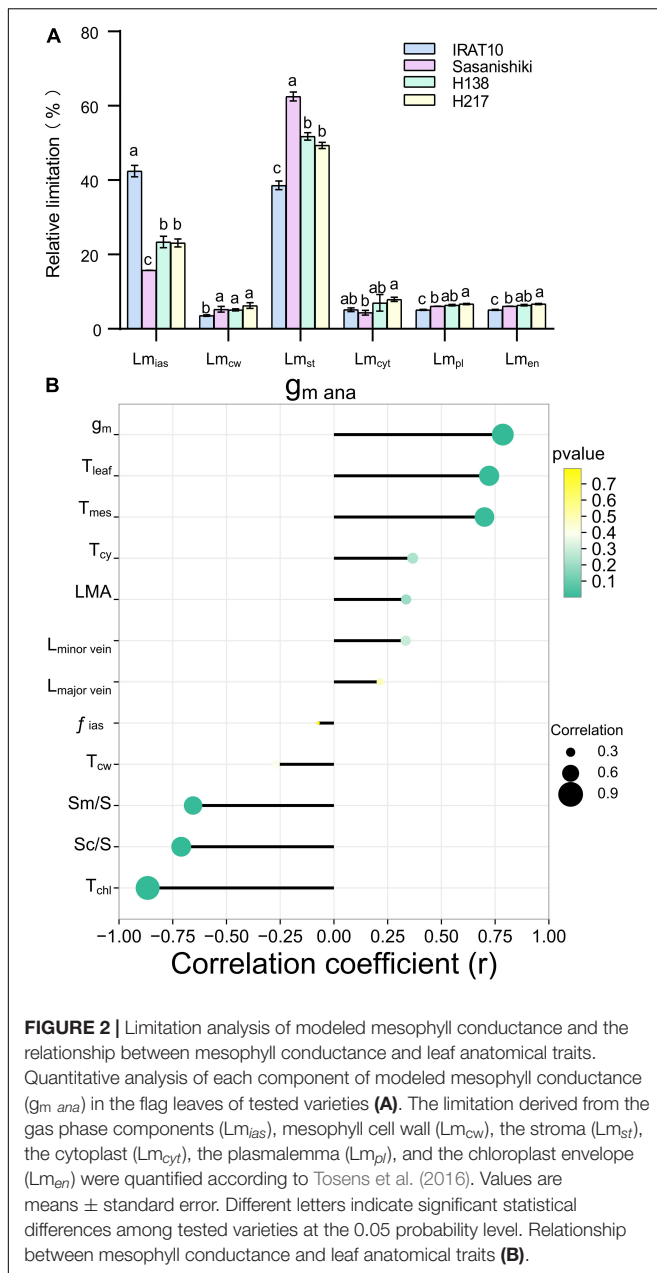
Mesophyll conductance ($g_{\text{m ana}}$), modeled from anatomical traits, was estimated according to the component diffusion conductance of the corresponding diffusion pathway, and the limitation of each component was calculated. The $g_{\text{m ana}}$ in flag

leaves of IRAT10, H138, and H217 was 33.3, 16.9, and 28.4%, respectively, was remarkably higher than that of Sasanishiki (0.081 mol m⁻² s⁻¹) (Table 2). The limitation derived from the gas phase components (L_{mias}), ranging from 15.7 to 42.4%, was lower than the total limitation from liquid phase components in all tested varieties (Figure 2A). A significantly higher limitation of gas-phase was recorded in IRAT10 flag leaves (42.4%) when compared with Sasanishiki (15.8%), H138 (23.4%), and H217 (23.1%). Relative to plasmalemma, cytoplasm, chloroplast envelope, and cell wall, limitations derived from stroma (L_{st}) were the main limitations among all components in all cultivars in the liquid phase. The L_{st} in IRAT10 (38.6%) flag leaves were significantly lower than that of Sasanishiki (62.5%), H138 (51.8%), and H217 (49.4%). Despite the value of g_{m} being dramatically higher than g_{mana} , a significant positive correlation ($r = 0.786$, $p < 0.01$) was observed between g_{mana} and g_{m} (Figure 2B). Also, significantly higher positive correlations were observed between g_{mana} and T_{leaf} ($r = 0.72$) and T_{mes} ($r = 0.7$). However, T_{chl} , $S_{\text{m/S}}$, and $S_{\text{c/S}}$ negative correlate with $g_{\text{m ana}}$.

Scanning electron microscope results showed that the maximum area of the open stomatal pore (a_{max}) of IRAT10 flag leaves on the adaxial side and the abaxial side was the largest (28.5, 23.4 μm²), and H138 having the smallest (17.5, 15.3 μm²) (Figure 3 and Supplementary Figure 3). The variation of stomatal density on the adaxial side of H138 (701 NO. mm⁻²) was significantly higher than that of IRAT10, Sasanishiki, and H217. The variation of stomatal density on the adaxial side ranged from 611 (H217) to 778 NO. mm⁻² (IRAT10). Maximum theoretical stomatal diffusive conductance (g_{Smax}) was calculated from stomatal density and stomatal area, and the total g_{Smax} was the sum of the adaxial and abaxial sides. The total g_{Smax} in the flag leaves of IRAT10, H138, and H217 was higher than that of Sasanishiki (1.33 mol m⁻² s⁻¹).

Photosynthetic Capacity

Relative to Sasanishiki flag leaves (25.1 μmol m⁻² s⁻¹), IRAT10, H138, and H217 have higher CO₂ assimilation (A_{n}) of 29.1, 27.5, and 29.1 μmol CO₂ m⁻² s⁻¹, respectively, at the heading stage (Figure 4). Stomatal conductance (g_{s}), estimated from the gas exchange, in IRAT10, H138, and H217 flag leaves, were 99, 30, and 26%, respectively, significantly higher than Sasanishiki (554 mmol m⁻² s⁻¹). Intercellular CO₂ concentration (C_{i}) in flag leaves of IRAT10, H138, and H217 were 7, 6.9, and 5.9%, respectively, significantly higher than Sasanishiki (309 μmol mol⁻²). Mesophyll conductance (g_{m}) was estimated from the gas exchange and fluorescence methods to show the CO₂ diffusion within the mesophyll cell level. Mesophyll conductance in flag leaves of H217, IRAT10, and H138 were 92, 88, and 58%, respectively, significantly higher than Sasanishiki (0.26 mol m⁻² s⁻¹). Hence, CO₂ concentration within the chloroplast (C_{c}) in flag leaves of IRAT10 (269 μmol mol⁻²), H138 (263 μmol mol⁻²), and H217 (268 μmol mol⁻²) were remarkably higher than Sasanishiki (221 μmol mol⁻²). A significant higher electron transport rate (J) was observed in IRAT10 (190 μmol m⁻² s⁻¹), H138 (185 μmol m⁻² s⁻¹), and H217 (189 μmol m⁻² s⁻¹) flag leaves than in Sasanishiki (173 μmol m⁻² s⁻¹).



Since a higher electron transport rate was recorded in H138 and H217, genes related to photosynthesis were checked. Genes encoding light-harvesting chlorophyll a/b protein at PSII and PSI, *Lhcb1*, *Lhcb2*, *Lhcb3*, *Lhca1*, *Lhca2*, and *Lhca3* were significantly upregulated in H138 and H217 than in Sasanishiki and IRAT10 at the heading stage (Supplementary Figure 4). The expression level of genes encoding PSII and PSI core subunit, *psbA*, *psbD*, and *psaA*, as well as genes encoding oxygen-evolving enhancer protein 1, *psbO*, were also upregulated in H138 and H217. This facilitates a better delivery in the electronic transport chain.

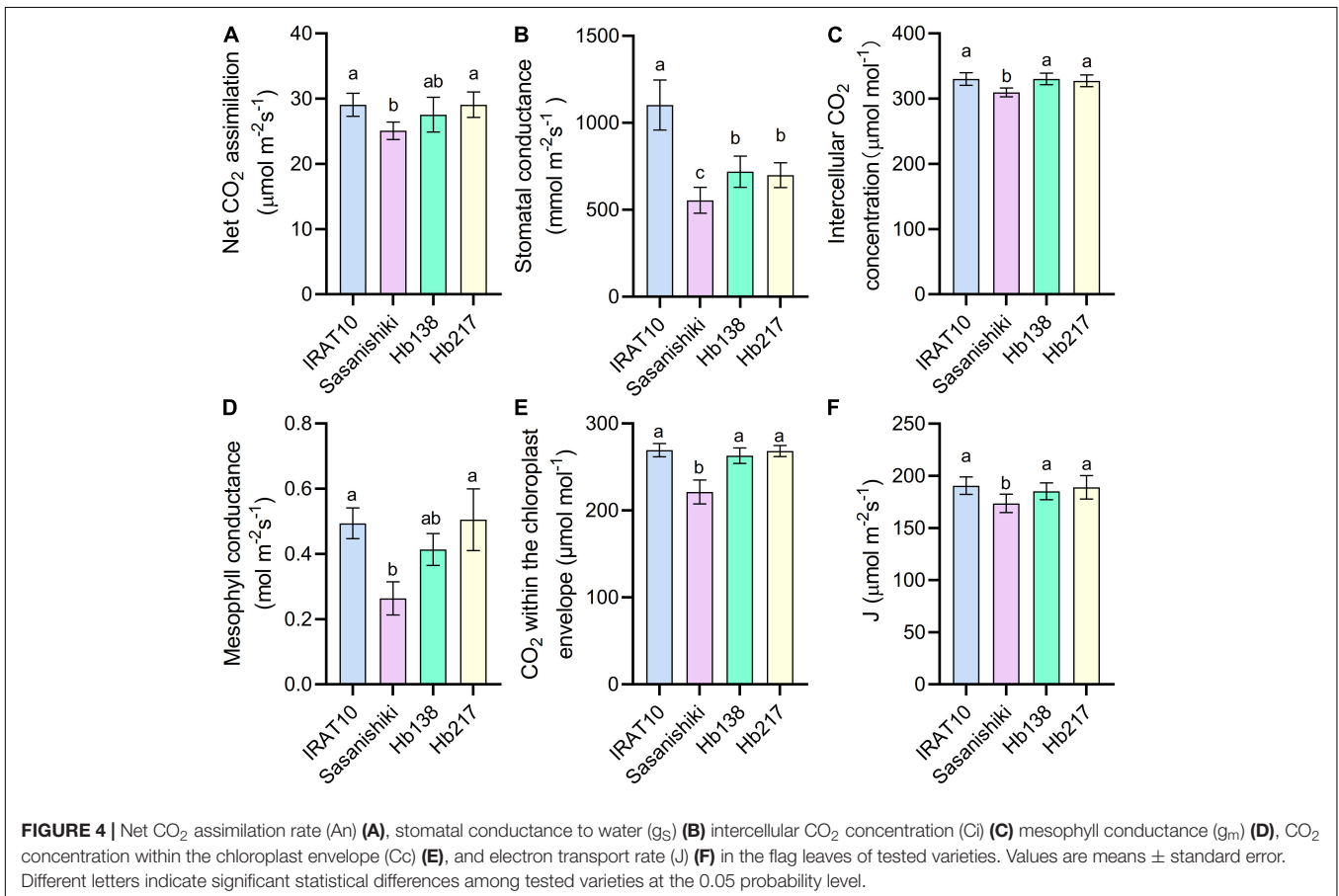
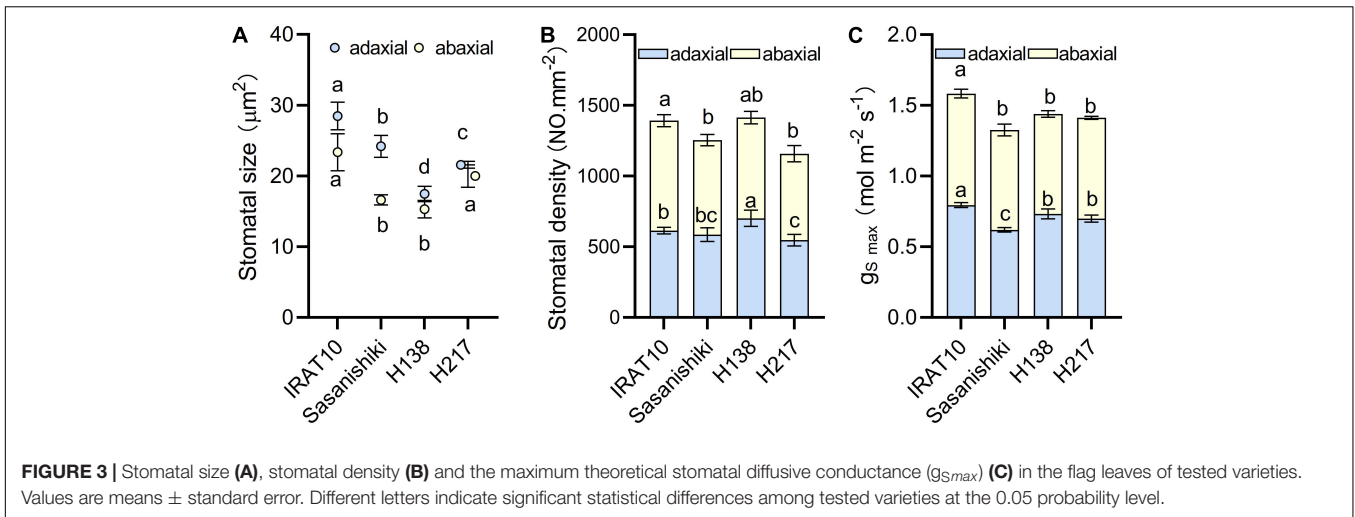
Significant higher chlorophyll content, N content, and RuBP content were observed in IRAT10 (3.3 mg g⁻¹, 3.3 mg g⁻¹, 83.2 ng g⁻¹), H138 (3.2 mg g⁻¹, 3.4 mg g⁻¹, 85.1 ng g⁻¹),

and H217 (3.2 mg g⁻¹, 3.5 mg g⁻¹, 82.4 ng g⁻¹) flag leaves compared to Sasanishiki (2.9 mg g⁻¹, 2.9 mg g⁻¹, 74.5 ng g⁻¹) (Figure 5). However, Rubisco content and Rubisco activity have no difference among tested varieties. The 3-phosphoglycerate (PGA) content in IRAT10 (845 ng g⁻¹), H138 (921 ng g⁻¹), and H217 (908 ng g⁻¹) flag leaves were significantly higher than in Sasanishiki (773 ng g⁻¹).

Anatomical traits and biochemical traits and CO₂ diffusion traits were selected to explore the relationship between them and An. Significant higher positive correlations were observed for An with J ($r = 0.85$), chlorophyll content ($r = 0.79$), g_m ($r = 0.74$), $NO_{\text{mescell}}/A_{\text{cross}}$ ($r = 0.80$), A_{mes} ($r = 0.72$), N ($r = 0.75$), Cc ($r = 0.70$), $g_{m \text{ ana}}$ ($r = 0.66$), RuBP ($r = 0.63$), A_{cross} ($r = 0.62$), Ci ($r = 0.52$), and g_s ($r = 0.45$) (Figure 6A). Significant negative correlations were found between T_{chl} and An, cause T_{chl} was the main factor that constrains CO₂ diffusion within mesophyll cells. Results from the structural equation model showed that mesophyll cell number has positive direct and indirect influences on An (Figure 6B). Another leaf anatomy trait that exerts an indirect influence on An was chloroplast thickness. The corresponding thickness of each component in the CO₂ diffusion pathways has direct effects on g_m . In tested rice, T_{chl} in the CO₂ diffusion pathways at the liquid phase was much thicker than other components.

DEGs Annotation and Functional Categorization

The KOG enrichment analysis was performed on the DEGs obtained from five pairwise comparisons of transcriptomes (Figure 7). Genes related to cell cycle control, cell division, and chromosome partitioning analyzed primarily, due to differences in mesophyll cell anatomy, were observed between Sasanishiki and IRAT10, H138, and H217. A total of 61 genes in this classification were observed in the five pairwise comparisons of transcriptomes. Five common DEGs were recorded in comparisons; IRAT10 vs. Sasanishiki, Sasanishiki vs. H138, and Sasanishiki vs. H217. They are *LOC_Os02g04080* (chromosome segregation protein *sudA*, putative, and expressed), *LOC_Os08g41070* (retrotransposon protein, putative, unclassified, and expressed), *LOC_Os09g27700* (microtubule-associated protein, putative, and expressed), *LOC_Os11g44014* (retrotransposon protein, putative, unclassified, and expressed), *LOC_Os12g20324* (cyclin-A1, putative, and expressed) (Figure 7B). Additionally, DEGs *LOC_Os02g27850* (retrotransposon protein, putative, unclassified, and expressed), *LOC_Os05g10580* (cullin family domain-containing protein, putative, and expressed), *LOC_Os06g44040* (DOMON domain-containing protein, and expressed), *LOC_Os07g10070* (retrotransposon protein, putative, unclassified, and expressed), and *LOC_Os11g47410* (retrotransposon protein, putative, unclassified, and expressed) were recorded in comparisons IRAT10 vs. Sasanishiki, IRAT10 vs. H138, and IRAT10 vs. H217. Cyclins and cyclin-dependent kinases (CDKs) are positive regulators of cell proliferation (Fisher et al., 2012). *LOC_Os12g20324* in H138 and H217 were inherited



from their parent IRAT10 and were expressed higher than their parent Sasanishiki (Figure 7C). However, *LOC_Os11g13860* (cyclin-dependent kinase, putative, and expressed) were lowly expressed in H138 and H217. The *LOC_Os08g42600* (*OsRBR1*) in H138 and H217 were inherited from their parent IRAT10 and were lowly expressed, which may contribute to small mesophyll cells and larger mesophyll cell numbers in H138 and H217 flag leaves.

DISCUSSION

Higher Assimilation in Selected Rice Recombinant Inbred Lines and Related Traits

Leaves exposed to complex environmental conditions of different temperatures and different irradiances inside the canopy often

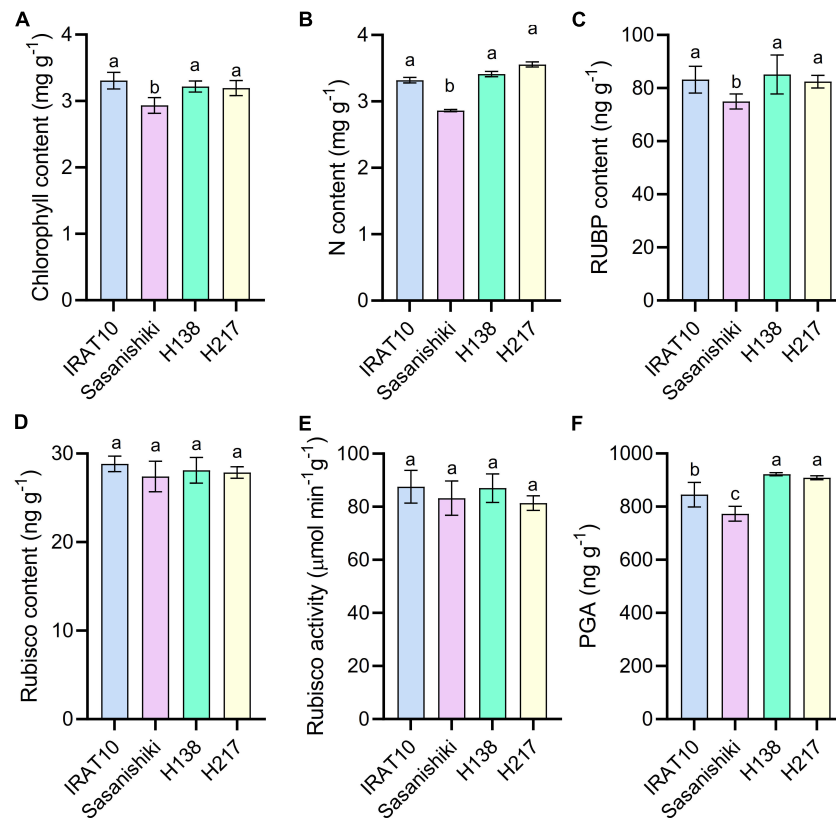


FIGURE 5 | Chlorophyll content (A), N content (B), RuBP content (C), Rubisco content (D), Rubisco activity (E), and PGA content (F) in the flag leaves of tested varieties. Values are means \pm standard error. Different letters indicate significant statistical differences among tested varieties at the 0.05 probability level.

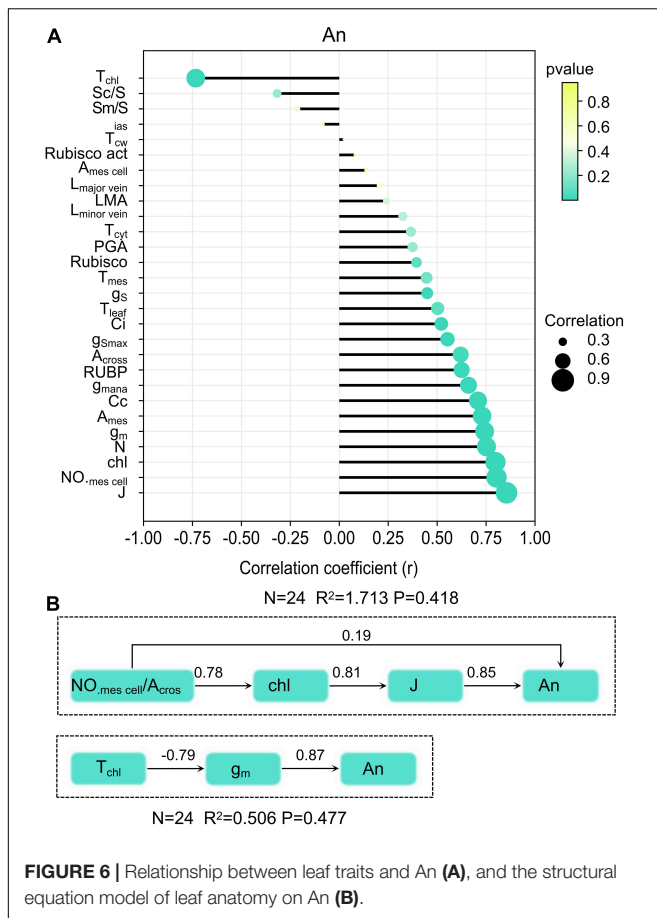
show dramatically different photosynthetic properties (Huang et al., 2021). Additionally, leaf ontogeny also affects leaf photosynthetic performance (Bielczynski et al., 2017). However, higher A_n in flag leaves of IRAT10, H138, and H217 than in Sasanishiki is determined by genotype, because similar trends were recorded two years at the heading stage (data measured in 2019 years are shown in **Supplementary Figure 5**). Increasing photosynthetic rates of individual leaves within the canopy has become an important strategy for increases in crop yield potential and productivity at the condition of canopy architecture close to optimal, especially in rice (Peter, 2000; Hubbart et al., 2007). Our results provide affirmative support for this strategy, higher yields were recorded in IRAT10, H138, and H217 compared to Sasanishiki (**Supplementary Table 2**). Thus, understanding the underlying traits that drive higher A_n in selected recombinant inbred lines is crucial.

Higher stomatal conductance (g_s) and mesophyll conductance (g_m) in flag leaves were observed in IRAT10, H138, and H217 compared to Sasanishiki, though differences existed in achieving higher g_s and g_m among tested varieties. This significantly facilitates higher CO_2 concentration in intercellular spaces, as well as at the carboxylation site, higher C_i and C_c were observed in IRAT10, H138, and H217 (**Figure 4**). Meanwhile, higher chlorophyll content and J were recorded in IRAT10, H138, and H217 flag leaves than in Sasanishiki, which would facilitate RuBP

regeneration, higher RuBP were recorded in IRAT10, H138, and H217 flag leaves (**Figure 5C**). Though N content in IRAT10, H138, and H217 flag leaves was higher than in Sasanishiki, no difference was observed in Rubisco content and activity among tested varieties (**Figures 5A,D,E**). The limitation of Rubisco activity primarily occurs at low intercellular CO_2 concentrations (Sharkey et al., 2007; Parry et al., 2013; von Caemmerer, 2020). A higher concentration of CO_2 and the content of RuBP at the active site of Rubisco are possibly resisting limitations from Rubisco (Parry et al., 2013; Lin et al., 2014; Sharwood, 2017). In our study, higher RuBP content together with higher CO_2 concentration at the carboxylation site in IRAT10, H138, and H217 flag leaves promoted CO_2 assimilation (**Figure 8**).

Target to Modify Leaf Anatomy for Achieving Higher Assimilation in Rice

Leaf anatomy, exerting influence on light use efficiency and CO_2 diffusion, is considered to have dramatic potential for photosynthesis performance increase. Also, increase cell density in the mesophyll of Arabidopsis leaf does increase leaf photosynthetic capacity (Lehmeier et al., 2017). Our result showed that $NO_{mescell}/A_{cross}$ exert positive influences on A_n through chlorophyll content (**Figure 6B**). Higher chlorophyll content and larger antenna size could intercept and absorb more



light energy (Ort et al., 2015). In this study, IRAT10, H138, and H217 have higher mesophyll cell numbers when compared to Sasanishiki flag leaves. Simultaneously, higher chlorophyll content and expression of genes encoding the light-harvesting protein of PSII and PSI (*Lhcb1*, 2, 3 and *Lhca1*, 2, 3) were recorded in IRAT10, H138, and H217, which facilitates light use efficiency. Better light use efficiency may facilitate RuBP regeneration and promotes CO₂ assimilation. Fortunately, cell density can be manipulated by modifying cell cycle-associated genes. Retinoblastoma-related gene, *RBR1*, plays a central role in regulating gene expression, endoreduplication, the number, size, and death (Sabelli et al., 2013). In Arabidopsis, suppression of *RBR1* can be used to generate organs with smaller cells in leaves (Lehmeier et al., 2017). Gene *OsRBR1* (*LOC_OS08g42600*) in H138 and H217 were inherited from IRAT10 and were lowly expressed than IRAT10 (Figure 7B). This might cause a larger number of small mesophyll cells in H138 and H217 flag leaves. Hence, mesophyll cell density will be a good target to improve photosynthesis in engineering leaf anatomy.

Relationship of g_m to Leaf Anatomy Traits in Rice

Harley's methods and anatomical methods were used to estimate g_m as accurately as possible. A significantly higher positive correlation was found between the two methods, suggesting that

somehow the variations in g_m among the tested varieties are at least partly related to the differences in the thickness of the structures involved in CO₂ diffusion pathways (Tomas et al., 2013). Despite the same variation of g_m in tested breeds being observed, a significantly lower value was recorded in anatomy methods compared to Variable J methods. This indicates that the resistance derived from anatomy structure is limited or is underestimated, more properties related to each component need to be considered in modeling g_m . For one reason, the distance from the bottom of the bulliform cell to the outermost mesophyll cell is about half the distance between the two epidermis cells due to the presence of bulliform cells. In this paper, the averaged distance of the two distances mentioned above was taken as the mesophyll layer thickness. Additionally, g_m cannot be regarded as a pure diffusion component, g_m is essentially a flux-weighted quantity, the amount of CO₂ diffused from mitochondria to chloroplasts at the process of respiration and photorespiration had to be considered in g_m estimation (Tholen et al., 2012).

Considering only diffusional component, limitation derived from the liquid phase components was the main factor constraining CO₂ diffusion in tested varieties, which is consistent with the results found in cotton and gymnosperms (Han et al., 2018; Carriqui et al., 2020). Interestingly, T_{chl} was the main factor restricting CO₂ diffusion in liquid-phase in tested rice, rather than T_{cw} . The corresponding thickness of each component in the CO₂ diffusion pathways has direct effects on mesophyll conductance. In tested rice, the chloroplast thickness was significantly thicker than the cell wall thickness of mesophyll cells. Cell wall resistance to CO₂ diffusion depends on physical properties like cell wall thickness, porosity, and tortuosity. Meanwhile, cell wall porosity varied with T_{cw} , and thinner cell wall at mesophyll cells may with a higher cell wall porosity Tosens et al., 2016. Cell wall thickness in tested varieties was thinner than that reported in cotton and gymnosperms (Han et al., 2018; Carriqui et al., 2020). Additionally, cell wall thickness, conformation, and complexity can be modified by changing cell wall components and biochemical properties, which exert dramatic influences on CO₂ diffusion through the cell wall (Carriqui et al., 2020). Hence, T_{cw} may play only a minor role in constraining CO₂ diffusion in rice flag leaves. Chloroplast thickness was the dominant factor restricting CO₂ diffusion within mesophyll cells rather than cell wall thickness.

Previously, LMA was reported as negatively correlated with g_m , but this relationship has been redefined (Ren et al., 2019). They reviewed that an increase in LMA dramatically improves Sm and Sc when LMA is less than 100 g m⁻², but plays only a minor role when it exceeds 100 g m⁻², even higher LMA reduces the f_{ias} , Sc/Sm, and g_m values (Ren et al., 2019). In our study, LMA was far less than 100 g m⁻² in all tested varieties, with IRAT10 having the highest and H217 having the lowest, but we did not observe an increase in Sm and Sc consistent with LMA (Tables 1, 2). On the contrary, Sm and Sc in IRAT10 flag leaves were significantly lower than that of Sasanishiki, H138, and H217. This is mainly due to IRAT10 having a larger mesophyll cell size and more mesophyll cell numbers, but lower intercellular airspace within leaves

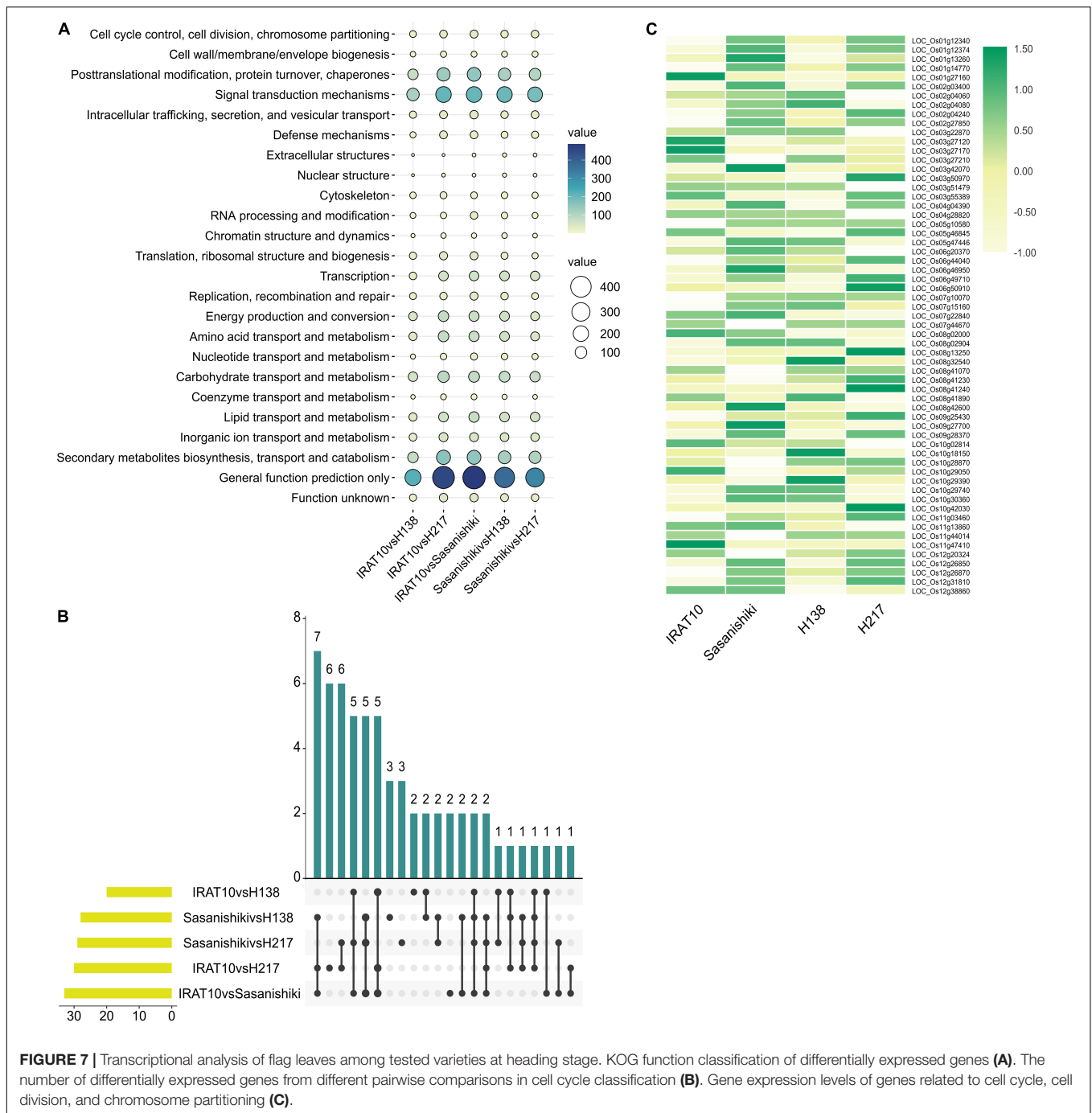
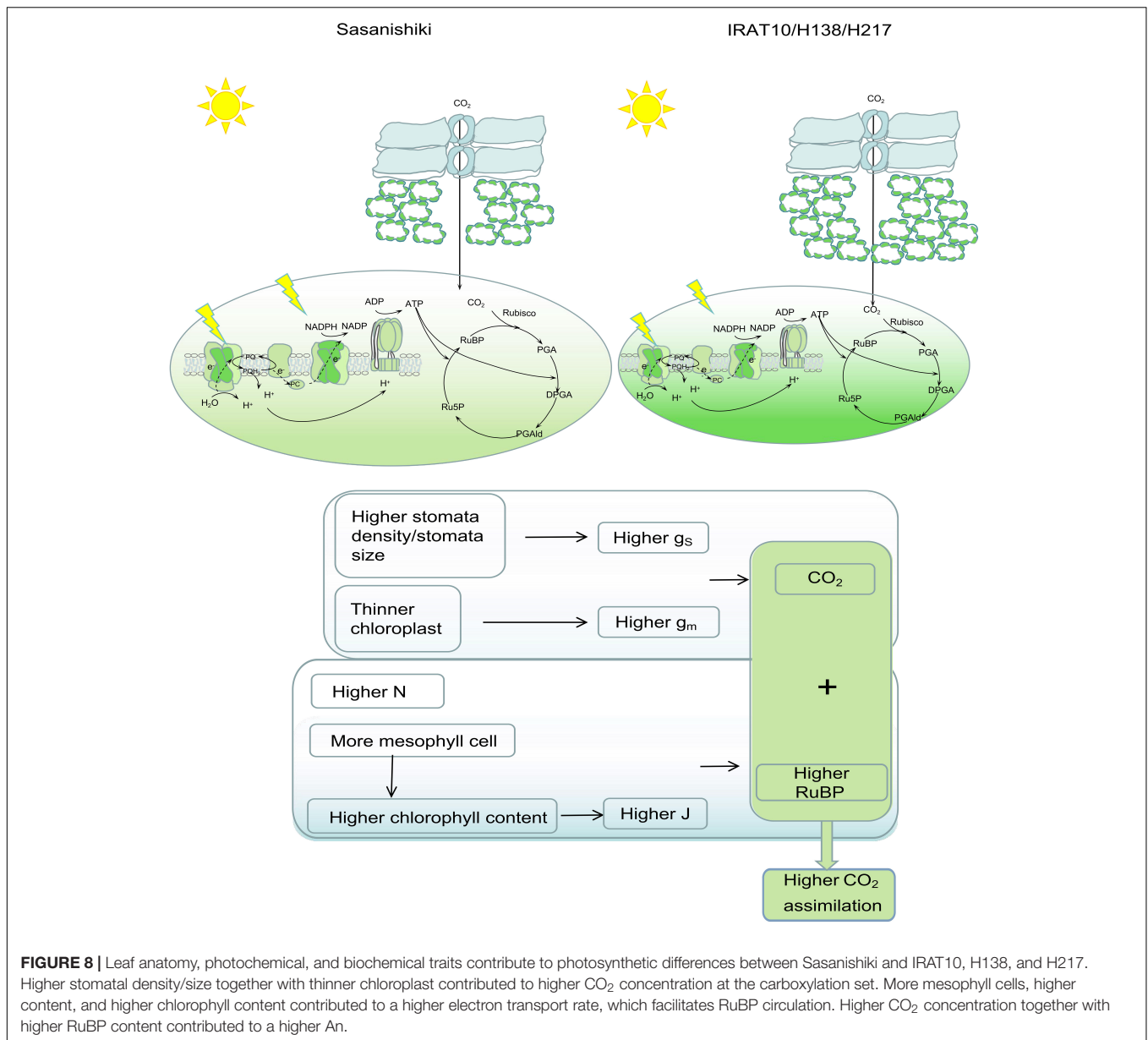


FIGURE 7 | Transcriptional analysis of flag leaves among tested varieties at heading stage. KOG function classification of differentially expressed genes (A). The number of differentially expressed genes from different pairwise comparisons in cell cycle classification (B). Gene expression levels of genes related to cell cycle, cell division, and chromosome partitioning (C).

(Tables 1, 2). The result indicated that rice, different from cotton and gymnosperms, is a special species. An increase in LMA may lead to the dense packing of mesophyll cells, which dramatically reduces Sm/S and inevitably decreases g_m (Flexas et al., 2008; Niinemets et al., 2009; Sarathi et al., 2016). Reasonably, we observed a significant negative correlation of Sm and Sc with g_m . Also, the slice photos were shown in **Supplementary Figure 6**. Hence, the difference among tested varieties can be mainly explained by the difference observed in chloroplast thickness.

In summary, we analyzed the photosynthetic capacity and corresponding constraints on CO_2 assimilation in selected rice recombinant inbred lines, H138 and H217, compared to their parent. Higher chlorophyll content and electron transport rate (mediated by higher mesophyll cell numbers), together with higher mesophyll conductance (mediated by chloroplast thickness), contributed to higher An in flag leaves of H138 and H217 at the heading stage. Chloroplast thickness was the dominant factor restricting CO_2 diffusion within mesophyll cells rather than cell wall thickness. Mesophyll cell



density will be a good target to improve photosynthesis in engineering leaf anatomy.

DATA AVAILABILITY STATEMENT

The datasets presented in this study can be found in online repositories. The names of the repository/repositories and accession number(s) can be found below: NCBI; PRJNA834750.

AUTHOR CONTRIBUTIONS

DM and JW designed experiments. FZ, LZ, and YL performed experiments. FZ, LZ, and GW analyzed data and compiled

figures. FZ and JW wrote the manuscript. DM edited the final manuscript. All authors contributed to the article and approved the submitted version.

FUNDING

This research was supported by the Shenyang Science and Technology Planning Project (21-110-3-08).

SUPPLEMENTARY MATERIAL

The Supplementary Material for this article can be found online at: <https://www.frontiersin.org/articles/10.3389/fpls.2022.915050/full#supplementary-material>

REFERENCES

- Barroco, R. M., Peres, A., Droual, A. M., De Veylder, L., Nguyen le, S. L., De Wolf, J., et al. (2006). The cyclin-dependent kinase inhibitor *Oryza*:KRP1 plays an important role in seed development of rice. *Plant Physiol.* 142, 1053–1064. doi: 10.1104/pp.106.087056
- Bielczynski, L. W., Lacki, M. K., Hoefnagels, I., Gambin, A., and Croce, R. (2017). Leaf and plant age affects photosynthetic performance and photoprotective capacity. *Plant Physiol.* 175, 1634–1648. doi: 10.1104/pp.17.00904
- Carriqui, M., Nadal, M., Clemente-Moreno, M. J., Gago, J., Miedes, E., and Flexas, J. (2020). Cell wall composition strongly influences mesophyll conductance in gymnosperms. *Plant J.* 103, 1372–1385. doi: 10.1111/tpj.14806
- Evans, J. R. (2021). Mesophyll conductance: walls, membranes and spatial complexity. *New Phytol.* 229, 1864–1876. doi: 10.1111/nph.16968
- Evans, J. R., Ca Emmerer, S. V., Setchell, B. A., and Hudson, G. S. (1994). The relationship between CO₂ transfer conductance and leaf anatomy in transgenic tobacco with a reduced content of Rubisco. *Aust. J. Plant Physiol.* 21:475.
- Evans, J. R., Kaldenhoff, R., Genty, B., and Terashima, I. (2009). Resistances along the CO₂ diffusion pathway inside leaves. *J. Exp. Bot.* 60, 2235–2248. doi: 10.1093/jxb/erp117
- Fisher, D., Krasinska, L., Coudreau, D., and Novak, B. (2012). Phosphorylation network dynamics in the control of cell cycle transitions. *J. Cell Sci.* 125(Pt 20), 4703–4711. doi: 10.1242/jcs.106351
- Flexas, J., Clemente-Moreno, M. J., Bota, J., Brodribb, T. J., Gago, J., Mizokami, Y., et al. (2021). Cell wall thickness and composition are involved in photosynthetic limitation. *J. Exp. Bot.* 72, 3971–3986. doi: 10.1093/jxb/erab144
- Flexas, J., Diaz-Espejo, A., Galmes, J., Kaldenhoff, R., Medrano, H., and Ribas-Carbo, M. (2007). Rapid variations of mesophyll conductance in response to changes in CO₂ concentration around leaves. *Plant Cell Environ.* 30, 1284–1298. doi: 10.1111/j.1365-3040.2007.01700.x
- Flexas, J., Ribas-Carbo, M., Diaz-Espejo, A., Galmes, J., and Medrano, H. (2008). Mesophyll conductance to CO₂: current knowledge and future prospects. *Plant Cell Environ.* 31, 602–621. doi: 10.1111/j.1365-3040.2007.01757.x
- Gilbert, M. E., Pou, A., Zwieniecki, M. A., and Holbrook, N. M. (2012). On measuring the response of mesophyll conductance to carbon dioxide with the variable J method. *J. Exp. Bot.* 63, 413–425. doi: 10.1093/jxb/err288
- Han, J., Lei, Z., Flexas, J., Zhang, Y., Carriqui, M., Zhang, W., et al. (2018). Mesophyll conductance in cotton bracts: anatomically determined internal CO₂ diffusion constraints on photosynthesis. *J. Exp. Bot.* 69, 5433–5443. doi: 10.1093/jxb/ery296
- Harley, P. C., Loreto, F., Marco, G. D., and Sharkey, T. D. (1992). Theoretical considerations when estimating the mesophyll conductance to CO₂ flux by analysis of the response of photosynthesis to CO₂. *Plant Physiol.* 98, 1429–1436.
- He, W., Adachi, S., Sage, R. F., Ookawa, T., and Hirasawa, T. (2017). Leaf photosynthetic rate and mesophyll cell anatomy changes during ontogenesis in backcrossed indica x japonica rice inbred lines. *Photosynth. Res.* 134, 27–38. doi: 10.1007/s11120-017-0403-x
- Huang, X., Wang, Z., Huang, J., Peng, S., and Xiong, D. (2021). Mesophyll conductance variability of rice aquaporin knockout lines at different growth stages and growing environments. *Plant J.* 107, 1503–1512. doi: 10.1111/tpj.15397
- Hubbart, S., Peng, S., Horton, P., Chen, Y., and Murchie, E. H. (2007). Trends in leaf photosynthesis in historical rice varieties developed in the Philippines since 1966. *J. Exp. Bot.* 58, 3429–3438. doi: 10.1093/jxb/erm192
- Lawson, T., Kramer, D. M., and Raines, C. A. (2012). Improving yield by exploiting mechanisms underlying natural variation of photosynthesis. *Curr. Opin. Biotechnol.* 23, 215–220. doi: 10.1016/j.copbio.2011.12.012
- Lehmeier, C., Pajor, R., Lundgren, M. R., Mathers, A., Sloan, J., Bauch, M., et al. (2017). Cell density and airspace patterning in the leaf can be manipulated to increase leaf photosynthetic capacity. *Plant J.* 92, 981–994. doi: 10.1111/tpj.13727
- Li, Y., Gao, Y., Xu, X., Shen, Q., and Guo, S. (2009). Light-saturated photosynthetic rate in high-nitrogen rice (*Oryza sativa* L.) leaves is related to chloroplastic CO₂ concentration. *J. Exp. Bot.* 60, 2351–2360. doi: 10.1093/jxb/erp127
- Liao, Y., Smyth, G. K., and Shi, W. (2014). featureCounts: an efficient general purpose program for assigning sequence reads to genomic features. *Bioinformatics* 30, 923–930. doi: 10.1093/bioinformatics/btt656
- Lin, M. T., Occhialini, A., Andralojc, P. J., Parry, M. A., and Hanson, M. R. (2014). A faster Rubisco with potential to increase photosynthesis in crops. *Nature* 513, 547–550. doi: 10.1038/nature13776
- Livak, K. J., and Schmittgen, T. D. (2001). Analysis of relative gene expression data using real-time quantitative PCR and the 2^{-ΔΔC_T} Method. *Methods* 25, 402–408. doi: 10.1006/meth.2001.1262
- Love, M. I., Huber, W., and Anders, S. (2014). Moderated estimation of fold change and dispersion for RNA-seq data with DESeq2. *Genome Biol.* 15:550. doi: 10.1186/s13059-014-0550-8
- Manter, D. K., and Kerrigan, J. (2004). A/C(i) curve analysis across a range of woody plant species: influence of regression analysis parameters and mesophyll conductance. *J. Exp. Bot.* 55, 2581–2588. doi: 10.1093/jxb/erh260
- Mathan, J., Singh, A., Jathar, V., and Ranjan, A. (2021). High photosynthesis rate in two wild rice species is driven by leaf anatomy mediating high Rubisco activity and electron transport rate. *J. Exp. Bot.* 72, 7119–7135. doi: 10.1093/jxb/erab313
- Niinemets, U., Wright, I. J., and Evans, J. R. (2009). Leaf mesophyll diffusion conductance in 35 Australian sclerophylls covering a broad range of foliage structural and physiological variation. *J. Exp. Bot.* 60, 2433–2449. doi: 10.1093/jxb/erp045
- Niinemets, Ü (2003). Controls on the emission of plant volatiles through stomata: a sensitivity analysis. *J. Geophys. Res.* 108:4211. doi: 10.1029/2002jd002626
- Ort, D. R., Merchant, S. S., Alric, J., Barkan, A., Blankenship, R. E., Bock, R., et al. (2015). Redesigning photosynthesis to sustainably meet global food and bioenergy demand. *Proc. Natl. Acad. Sci. U.S.A.* 112, 8529–8536. doi: 10.1073/pnas.1424031112
- Ouyang, W., Struik, P. C., Yin, X., and Yang, J. (2017). Stomatal conductance, mesophyll conductance, and transpiration efficiency in relation to leaf anatomy in rice and wheat genotypes under drought. *J. Exp. Bot.* 68, 5191–5205. doi: 10.1093/jxb/erx314
- Parry, M. A., Andralojc, P. J., Scales, J. C., Salvucci, M. E., Carmo-Silva, A. E., Alonso, H., et al. (2013). Rubisco activity and regulation as targets for crop improvement. *J. Exp. Bot.* 64, 717–730. doi: 10.1093/jxb/ers336
- Peguero-Pina, J. J., Siso, S., Flexas, J., Galmes, J., Garcia-Nogales, A., Niinemets, U., et al. (2017). Cell-level anatomical characteristics explain high mesophyll conductance and photosynthetic capacity in sclerophyllous Mediterranean oaks. *New Phytol.* 214, 585–596. doi: 10.1111/nph.14406
- Peter, H. (2000). Prospects for crop improvement through the genetic manipulation of photosynthesis: morphological and biochemical aspects of light capture. *J. Exp. Bot.* 51(suppl_1), 475–485. doi: 10.1093/jexbot/51.suppl_1.475
- Pons, T. L., Flexas, J., von Caemmerer, S., Evans, J. R., Genty, B., Ribas-Carbo, M., et al. (2009). Estimating mesophyll conductance to CO₂: methodology, potential errors, and recommendations. *J. Exp. Bot.* 60, 2217–2234. doi: 10.1093/jxb/erp081
- Ren, T., Weraduwage, S. M., and Sharkey, T. D. (2019). Prospects for enhancing leaf photosynthetic capacity by manipulating mesophyll cell morphology. *J. Exp. Bot.* 70, 1153–1165. doi: 10.1093/jxb/ery448
- Sabelli, P. A., Liu, Y., Dante, R. A., Lizarraga, L. E., Nguyen, H. N., Brown, S. W., et al. (2013). Control of cell proliferation, endoreduplication, cell size, and cell death by the retinoblastoma-related pathway in maize endosperm. *Proc. Natl. Acad. Sci. U.S.A.* 110, E1827–E1836. doi: 10.1073/pnas.1304903110
- Sarathi, M. W., Kim, S. J., Renna, L., Anozie, C. F., Sharkey, D. T., and Brandizzi, F. (2016). Pectin methylesterification impacts the relationship between photosynthesis and plant growth. *Plant Physiol.* 171, 833–848. doi: 10.1104/pp.16.00173
- Sartory, D. P., and Grobbelaar, J. U. (1984). Extraction of chlorophyll a from freshwater phytoplankton for spectrophotometric. *Hydrobiologia* 114, 117–187. doi: 10.1007/BF00031869
- Scafaro, A. P., Von Caemmerer, S., Evans, J. R., and Atwell, B. J. (2011). Temperature response of mesophyll conductance in cultivated and wild *Oryza* species with contrasting mesophyll cell wall thickness. *Plant Cell Environ.* 34, 1999–2008. doi: 10.1111/j.1365-3040.2011.02398.x
- Sharkey, T. D., Bernacchi, C. J., Farquhar, G. D., and Singsaas, E. L. (2007). Fitting photosynthetic carbon dioxide response curves for C(3) leaves. *Plant Cell Environ.* 30, 1035–1040. doi: 10.1111/j.1365-3040.2007.01710.x
- Sharwood, R. E. (2017). Engineering chloroplasts to improve Rubisco catalysis: prospects for translating improvements into food and fiber crops. *New Phytol.* 213, 494–510. doi: 10.1111/nph.14351

- Simkin, A. J., Lopez-Calcano, P. E., and Raines, C. A. (2019). Feeding the world: improving photosynthetic efficiency for sustainable crop production. *J. Exp. Bot.* 70, 1119–1140. doi: 10.1093/jxb/ery445
- Syvrtsen, J. P., Lloyd, J., Mcconchie, C., Kriedemann, P. E., and Farquhar, G. D. (2010). On the relationship between leaf anatomy and CO₂ diffusion through the mesophyll of hypostomatous leaves. *Plant Cell Environ.* 18, 149–157.
- Tholen, D., Ethier, G., Genty, B., Pepin, S., and Zhu, X. G. (2012). Variable mesophyll conductance revisited: theoretical background and experimental implications. *Plant Cell Environ.* 35, 2087–2103. doi: 10.1111/j.1365-3040.2012.02538.x
- Tomas, M., Flexas, J., Copolovici, L., Galmes, J., Hallik, L., Medrano, H., et al. (2013). Importance of leaf anatomy in determining mesophyll diffusion conductance to CO₂ across species: quantitative limitations and scaling up by models. *J. Exp. Bot.* 64, 2269–2281. doi: 10.1093/jxb/ert086
- Tosens, T., Niinemets, U., Vislap, V., Eichelmann, H., and Castro Diez, P. (2012a). Developmental changes in mesophyll diffusion conductance and photosynthetic capacity under different light and water availabilities in *Populus tremula*: how structure constrains function. *Plant Cell Environ.* 35, 839–856. doi: 10.1111/j.1365-3040.2011.02457.x
- Tosens, T., Niinemets, U., Westoby, M., and Wright, I. J. (2012b). Anatomical basis of variation in mesophyll resistance in eastern Australian sclerophylls: news of a long and winding path. *J. Exp. Bot.* 63, 5105–5119. doi: 10.1093/jxb/ers171
- Tosens, T., Nishida, K., Gago, J., Coopman, R. E., Cabrera, H. M., Carriqui, M., et al. (2016). The photosynthetic capacity in 35 ferns and fern allies: mesophyll CO₂ diffusion as a key trait. *New Phytol.* 209, 1576–1590. doi: 10.1111/nph.13719
- Valentini, R., Epron, D., Angelis, P. D., Matteucci, G., and Dreyer, E. (1995). In situ estimation of net CO₂ assimilation, photosynthetic electron flow and photorespiration in Turkey oak (*Q. cerris* L.) leaves: diurnal cycles under different levels of water supply. *Plant, Cell Environ.* 18, 631–640.
- Varet, H., Brillet-Gueguen, L., Coppee, J. Y., and Dillies, M. A. (2016). SARTools: a DESeq2- and edgeR-based R pipeline for comprehensive differential analysis of RNA-seq data. *PLoS One* 11:e0157022. doi: 10.1371/journal.pone.0157022
- von Caemmerer, S. (2020). Rubisco carboxylase/oxygenase: from the enzyme to the globe: a gas exchange perspective. *J. Plant Physiol.* 252, 153240. doi: 10.1016/j.jplph.2020.153240
- Xiong, D., and Flexas, J. (2018). Leaf economics spectrum in rice: leaf anatomical, biochemical, and physiological trait trade-offs. *J. Exp. Bot.* 69, 5599–5609. doi: 10.1093/jxb/ery322
- Xiong, D., Flexas, J., Yu, T., Peng, S., and Huang, J. (2017). Leaf anatomy mediates coordination of leaf hydraulic conductance and mesophyll conductance to CO₂ in *Oryza*. *New Phytol.* 213, 572–583. doi: 10.1111/nph.14186
- Zhang, G. H., Li, S. Y., Wang, L., Ye, W. J., Zeng, D. L., Rao, Y. C., et al. (2014). LSCHL4 from Japonica Cultivar, which is allelic to NAL1, increases yield of indica super rice 93-11. *Mol. Plant* 7, 1350–1364. doi: 10.1093/mp/ssu055
- Zhu, X. G., Long, S. P., and Ort, D. R. (2010). Improving photosynthetic efficiency for greater yield. *Annu. Rev. Plant Biol.* 61, 235–261. doi: 10.1146/annurev-arplant-042809-112206

Conflict of Interest: The authors declare that the research was conducted in the absence of any commercial or financial relationships that could be construed as a potential conflict of interest.

Publisher's Note: All claims expressed in this article are solely those of the authors and do not necessarily represent those of their affiliated organizations, or those of the publisher, the editors and the reviewers. Any product that may be evaluated in this article, or claim that may be made by its manufacturer, is not guaranteed or endorsed by the publisher.

Copyright © 2022 Zeng, Zhu, Wang, Liang, Ma and Wang. This is an open-access article distributed under the terms of the Creative Commons Attribution License (CC BY). The use, distribution or reproduction in other forums is permitted, provided the original author(s) and the copyright owner(s) are credited and that the original publication in this journal is cited, in accordance with accepted academic practice. No use, distribution or reproduction is permitted which does not comply with these terms.